Biomatter

ISSN: (Print) 2159-2535 (Online) Journal homepage: http://www.tandfonline.com/loi/kbim20

Influence of ECAP process on mechanical and corrosion properties of pure Mg and ZK60 magnesium alloy for biodegradable stent applications

Ehsan Mostaed, Maurizio Vedani, Mazdak Hashempour & Massimiliano Bestetti

To cite this article: Ehsan Mostaed, Maurizio Vedani, Mazdak Hashempour & Massimiliano Bestetti (2014) Influence of ECAP process on mechanical and corrosion properties of pure Mg and ZK60 magnesium alloy for biodegradable stent applications, Biomatter, 4:1, e28283, DOI: 10.4161/biom.28283

To link to this article: http://dx.doi.org/10.4161/biom.28283

Biomatter 4, e28283; February; © 2014 Landes Bioscience

Influence of ECAP process on mechanical and corrosion properties of pure Mg and ZK60 magnesium alloy for biodegradable stent applications

Ehsan Mostaed[1,*], Maurizio Vedani[1], Mazdak Hashempour[2], and Massimiliano Bestetti[2]

[1]Department of Mechanical Engineering; Politecnico di Milano; Milan, Italy; [2]Department of Chemistry; Materials and Chemical Engineering "Giulio Natta"; Politecnico di Milano; Milan, Italy

Keywords: Mg alloy, biodegradable, ECAP, ultra-fine grain, extrusion, corrosion

Equal channel angular pressing (ECAP) was performed on ZK60 alloy and pure Mg in the temperature range 150–250 °C. A significant grain refinement was detected after ECAP, leading to an ultrafine grain size (UFG) and enhanced formability during extrusion process. Comparing to conventional coarse grained samples, fracture elongation of pure Mg and ZK60 alloy were significantly improved by 130% and 100%, respectively, while the tensile strength remained at high level. Extrusion was performed on ECAP processed billets to produce small tubes (with outer/inner diameter of 4/2.5 mm) as precursors for biodegradable stents. Studies on extruded tubes revealed that even after extrusion the microstructure and microhardness of the UFG ZK60 alloy were almost stable. Furthermore, pure Mg tubes showed an additional improvement in terms of grain refining and mechanical properties after extrusion. Electrochemical analyses and microstructural assessments after corrosion tests demonstrated two major influential factors in corrosion behavior of the investigated materials. The presence of Zn and Zr as alloying elements simultaneously increases the nobility by formation of a protective film and increase the local corrosion damage by amplifying the pitting development. ECAP treatment decreases the size of the second phase particles thus improving microstructure homogeneity, thereby decreasing the localized corrosion effects.

Introduction

Nowadays, biomaterial technology is built on traditional permanent metallic materials including stainless steel, Nitinol and cobalt-chromium alloys. In particular, these inert materials are used as load-bearing implants for replacement of diseased or damaged tissues. However, some particular disadvantages, including physical irritation, chronic inflammatory inconvenience, long-term endothelial dysfunction and, more importantly in pediatric and adolescent patients, a second intervention is required for implant removal, causing adverse tissue reactions.[1-3]

More recently, biodegradable materials like magnesium and iron alloys have been proposed in medical science as a novel class of highly bioactive materials. That is, these materials are supposed to temporarily aid the healing process of a diseased tissue or organ and then they can progressively disappear by virtue of body fluids corrosion after a certain length of functional use, leading to simultaneous implant replacement through the surrounding tissue.[4-6]

Magnesium is one of the most promising candidates for biodegradable applications due to its biocompatibility as an essential element to human metabolism. Several studies have proven that the daily intake of Mg for a normal adult exceeds 300 mg and excessive magnesium cations possibly produces by degradation could be safely excreted in the urine.[6-11] However, the greatest limitation of Mg consists of its fast corrosion rate, especially in human body fluid containing chloride, giving rise to immature drop in mechanical integrity of the device before accomplishing its defined mission.[12,13] Over and above corrosion rate, critical hydrogen gas bubbles and alkalization resulting from corrosion of Mg in body fluid are also other problematic subjects in fast corrosion-rate processes, leading to accumulation of evolved hydrogen bubbles in gas pockets next to the implant and consequently, causing necrosis of tissues. However, if the corrosion rate of Mg implant can be suitably controlled, hydrogen evolution will not be rapid enough to cause critical subcutaneous bubbles, and the alkalization effect could be easily balanced by metabolic mechanisms in the human body.[14-16]

*Correspondence to: Ehsan Mostaed; Email: ehsan.mostaed@polimi.it
Submitted: 01/12/2014; Revised: 02/13/2014; Accepted: 02/18/2014; Published Online: 02/21/2014
http://dx.doi.org/10.4161/biom.28283

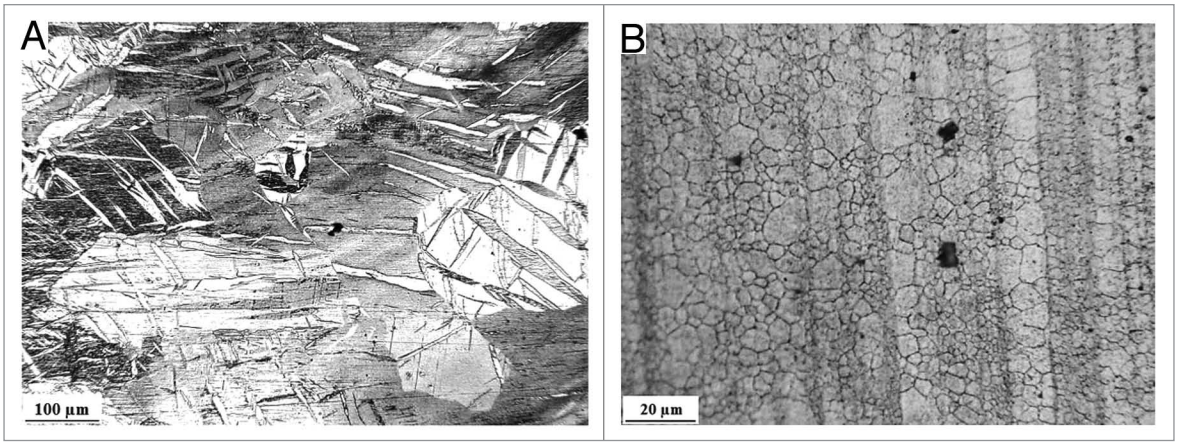

Figure 1. Microstructure of starting materials: MA (**A**) and AA (**B**).

A further challenging issue to be faced concerns mechanical properties. Generally, Mg alloys have lower mechanical properties than commonly used inert biomaterials. Considering stent applications, fracture of the stent strut during expansion also has to be avoided by enhancing alloy ductility. Therefore, controlling the corrosion rate to achieve a prolonged and uniform degradation of the device made by alloys with reasonable strength and ductility are key factors in the development of Mg implants and stents.[3,13,17]

In general, the most efficient approach to improve both mechanical properties and corrosion resistance of magnesium is adding specific alloying elements. There are two basic groups of Mg alloys namely those containing aluminum and the class of aluminum free alloys.[4,6-8] However, it has been reported that for the use in humans, aluminum free alloy systems are recommended since aluminum ions can combine with inorganic phosphates, causing a lack of phosphate in the human body.[4,18] On the other hand, it is cited that addition of rare earth (RE) elements (Ce, Y, etc.) could lead to hepatotoxicity and also excessive yttrium ions induces adverse effects on DNA transcription factors.[19,20]

It is therefore recognized that alloying elements must be carefully selected in order to meet the biocompatibility requirements.[7,14] Since it is demonstrated that Zn is an essential nutritive element and its ions can be absorbed without harming vital organs, this element could be the first choice among alloying elements. Zirconium, particularly in small amount, less that 0.8 wt%, is considered as a biocompatible element.[4,21,22] Accordingly, it is proven that introducing of Zn or Zr to pure Mg brought about improved mechanical properties and corrosion resistance as well as good cytocompatibility.[7,23,24]

In addition, several studies reported that grain refinement induced by processing techniques based on severe plastic deformation (SPD) is an effective approach to improve both mechanical and corrosion properties of Mg alloys due to Hall-Petch strengthening and homogeneous distribution of precipitates, respectively.[25-30] In recent years, as a novel metal forming process, Equal-channel angular pressing (ECAP) has been widely investigated on Mg alloys. However, those attempts generally cover works on mechanical properties assessments[28,31-33] and texture monitoring.[34-36] A couple of works have also investigated typical biomedical application based behavior of ECAPed Mg alloys.[9-13] Accordingly, a vacancy is felt about the bio-application based exploration of pure Mg, that is tried to be addressed in this work. Moreover, to the best of authors' knowledge, no systematic investigation of ECAP treated Mg based materials for stents application has been reported in the literature. Efforts have been put on elucidation of the primary steps of this area in this work.

Another objective of this work has been spotlighting the potential of ECAP process for supplying precursor materials for subsequent forming steps, such as extrusion, while keeping the favorable properties accessed by the very ECAP step, namely, ultrafined grain (UFG) structure. Interestingly, ECAP induced UFG structure, which has been an area of intense research and interest due to its excellent mechanical specifications, was retained even after ulterior treatments such as extrusion. In practice, this can be translated to a geometry close to final application (cylinder for stent in this case) with outstanding mechanical properties of a UFG structure. Further electrochemical measurements were also conducted to provide some basic information about the effect of such mechanical treatment on the corrosion resistance of the mater.

Results and Discussion

Microstructure

The microstructure of the as-received billets is shown in **Figure 1**. the MA (see the experimental part for reference to samples naming) sample possessed a quite coarse grain structure with average grain size of about 250 µm, whereas the AA sample featured a relatively finer and heterogeneous microstructure, with a bimodal grain size distribution made up of coarse grains of approximately 10–15 µm in size together with very fine grains of about 2–3µm (**Fig. 1B**).

In order to induce grain refinement in MA and AA billets without any cracking during ECAP, initial processing temperature had to be increased up to 275 °C and 250 °C for MA and AA, respectively. It has been demonstrated in an earlier work[30] that by

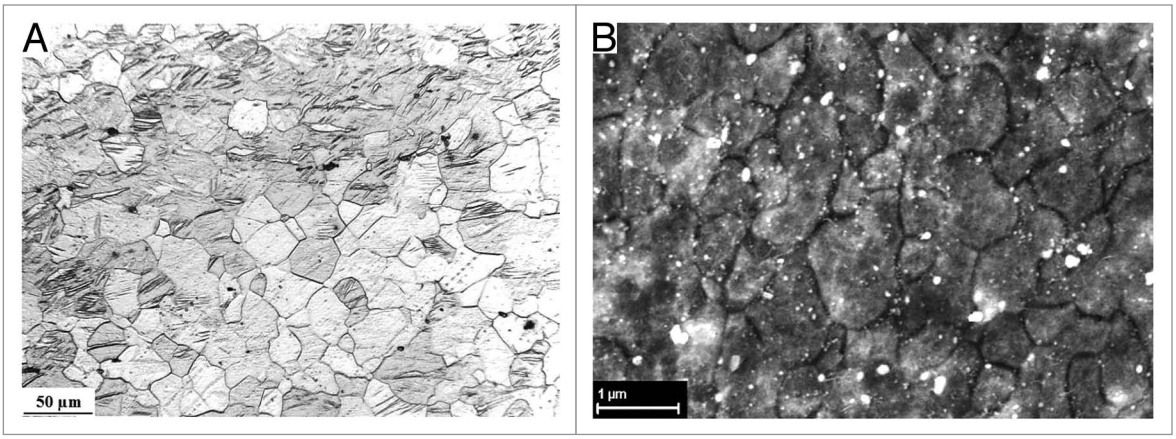

Figure 2. Microstructure of the samples after ECAP: ME (**A**) and AE (**B**).

increasing the initial temperature, the material formability was significantly improved without adversing the grain refinement effect, which could be completed in the following steps. In other words, the strategy of performing a first set of passes at relatively high temperature aimed at achieving a first substantial grain-size reduction and then completing the refinement in the required regime at lower temperature by subsequent set of passes revealed to be successful.

Figure 2A shows the microstructure of ME. It is apparent that the original coarse grained structure was significantly refined (compare with **Fig. 1A**), twinning was evident in the coarser grains also of the ECAP treated samples. The process was interrupted after 4 passes at 250 °C due to failure of specimens, preventing the achievement of a finer structure. Eventually, an equiaxed structure with grain size of 22 µm was achieved by ECAP in ME samples. In contrast, by a careful selection of ECAP processing temperatures and number of passes, a completely recrystallized structure by ultra-fine grains throughout the billet volume of the AE samples was achieved. The average grain size was of about 0.7 µm, as depicted in **Figure 2B**.

Mechanical properties

Microhardness

Figure 3 Shows the average Vickers microhardness measured on longitudinal sections of the samples before and after ECAP. It is clearly demonstrated that for pure Mg the hardness values remained almost constant with no significant improvement after ECAP processing. However, it is observed that for the ZK60 alloy investigated, hardness rose through ECAP, resulting in an improvement of about 18% (sample AE).

Tensile properties

The tensile stress vs. strain curves for as-received and ECAP processed samples are depicted in **Figure 4**. Tensile properties including, 0.2% proof stress (YS), ultimate tensile strength (UTS) and fracture elongation values (FE) drawn from these curves are also plotted in **Figure 5**. The data demonstrate that for the pure Mg (MA and ME samples, see **Figs. 4A and 5**) the yield stress did not change significantly after ECAP, while the UTS improved from 285 MPa up to a value of 326 MPa and a substantial increment of fracture elongation was measured as well, from

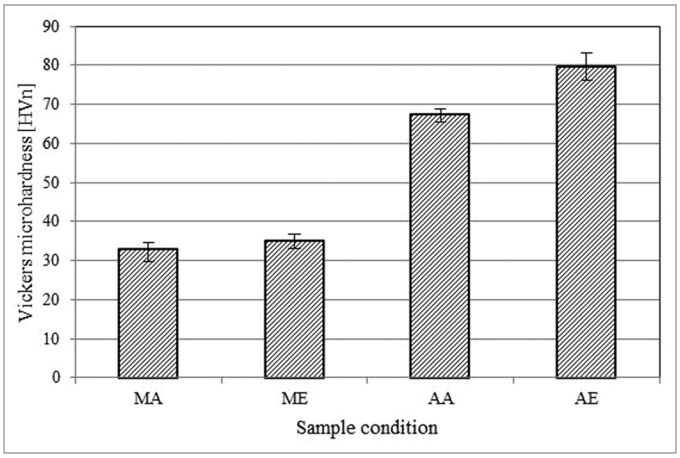

Figure 3. Average hardness of the investigated samples before and after ECAP.

an initial value of 4.4% to 10.3%. As shown in **Figures 1 and 2**, the grain size was considerably reduced by performing ECAP. Nevertheless, it is supposed that such grain size dependency is not the only factor influencing the yield strength and fracture elongation properties in Mg alloys. It is believed that mechanical behavior of the ECAP processed Mg would also be related to crystallographic texture modification in accordance with other literature reports.[37,38] In particular, when comparing the data of AA and AE materials it can be observed that the AE samples, despite their much finer grains featured lower YS and UTS than the as received alloy. It is suggested that this can be related to the dominant texture-softening effect over the grain size strengthening induced during ECAP passes at high temperatures.[39] On this basis, the elongation to failure of AE remarkably increased with an improvement of 100%, whereas the alloy still kept a relatively high tensile strength required for the stent application (**Figs. 4B and 5**).[40]

Extrusion

The ECAP processed samples, ME and AE, were then subjected to warm extrusion tests aimed at producing mini-tubes

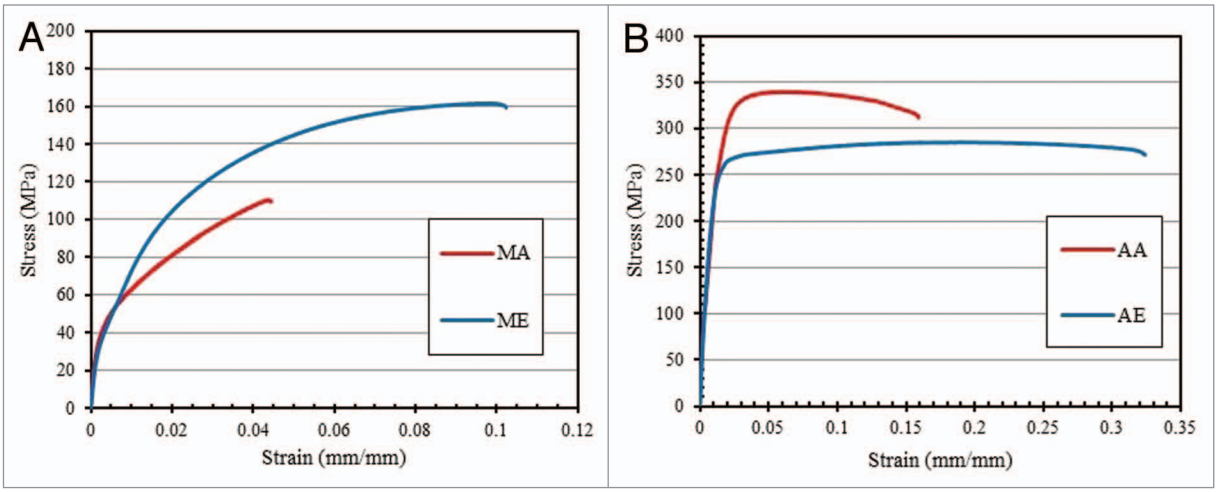

Figure 4. Tensile stress–strain curves measured at room temperature of the as-received and the ECAP processed Mg (**A**) and ZK60 alloy (**B**).

required for stent manufacturing. In order to evaluate the effect of grain refinement induced by ECAP on the mechanical properties of the final tubes and to comparatively evaluate the formability of the UFG materials, MA and AA were also processed as references for the extrusion tests.

It is verified that the high formability properties highlighted by the low extrusion load and absence of cracks are often inherited in UFG Mg alloys by the contribution of superplastic effects induced by the grain refinement.[41,42] Accordingly, extrusion for MEE could be performed at 230°C, while MAE, due to its coarser grain structure and lower formability could be safely extruded only at 300 °C. As a result, of the lower processing temperature, as shown in **Figure 6**, MEE sample shows much finer grain structure than MAE so that the combination of ECAP and low-temperature extrusion brought about a remarkable grain refinement in pure Mg to approximately 11µm. For the ZK60 alloy, as shown in **Figure 4B**, both conditions (AA and AE) featured a high plastic formability. Thus, AEE and AAE were successfully produced even at lower temperatures (150°C). **Figure 6C** suggests that in AAE sample a more homogeneous and finer equiaxed grain structure than in sample AA was obtained. It is worthy to note that no obvious grain growth was observed in AEE, certifying that UFG structure induced by ECAP process was maintained almost stable even after the extrusion at 150 °C (**Fig. 6D**).

For small-size tubes the mechanical properties were characterized by micro-hardness due to geometrical limitation of the samples. **Figure 7** shows the hardness profile measured along the cross section parallel to the extrusion direction of interrupted extrusion tests for Mg and ZK60 alloy samples. All curves indicate a gradual increase in hardness from billet region to extruded tube region.

From **Figure 7A and B** it can be understood that during the extrusion of AEE and MEE samples, when the billets were kept inside the die at high temperature a drop in hardness occurred when compared with values of ECAP processed billets. However, this gap was totally counterbalanced by the effect of plastic deformation during extrusion. Moreover, AEE and MEE samples always showed higher hardness values in all tested regions than of the corresponding AAE and MAE samples confirming that the improved properties inherited from ECAP are also kept after extrusion.

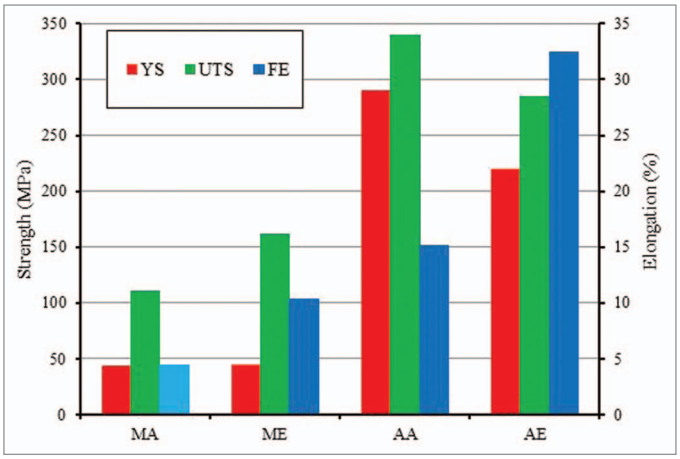

Figure 5. Tensile properties of Mg and ZK60 alloy as a function of samples condition. YS: tensile yield strength; UTS: ultimate tensile strength; FE: fracture elongation.

Corrosion

Electrochemical studies

Figure 8 shows the OCP measurement results of AA, AE, MA, and ME samples. As can be seen by the OCP plot, establishment of the steady-state did not happen before 12 h for pure Mg samples, based on which observation, an extra time was allowed (6 h) to ascertain a steady trend. For alloyed samples however, steady manner was established faster, within four hours. To keep the uniformity in all experiments, an 18 h period was allowed for OCP measurement of all samples.

Two distinct levels of OCP values can be recognized according to this plot referring to the composition of the metals. More

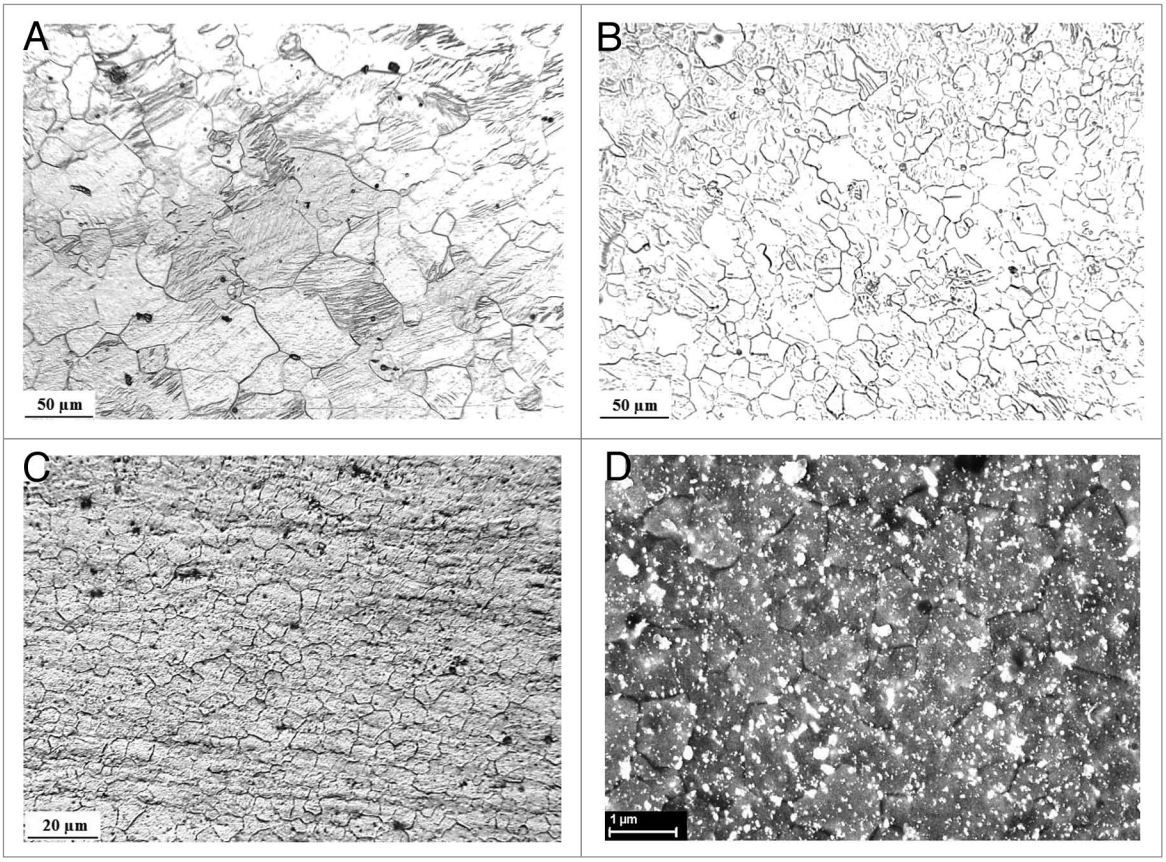

Figure 6. Representative micrographs of the mini-tube grain structure after extrusion for Mg and ZK60alloy at different temperatures. (**A**) MAE at 300 °C, (**B**) MEE at 230 °C, (**C**) AAE at 150 °C, (**D**) AEE at 150 °C.

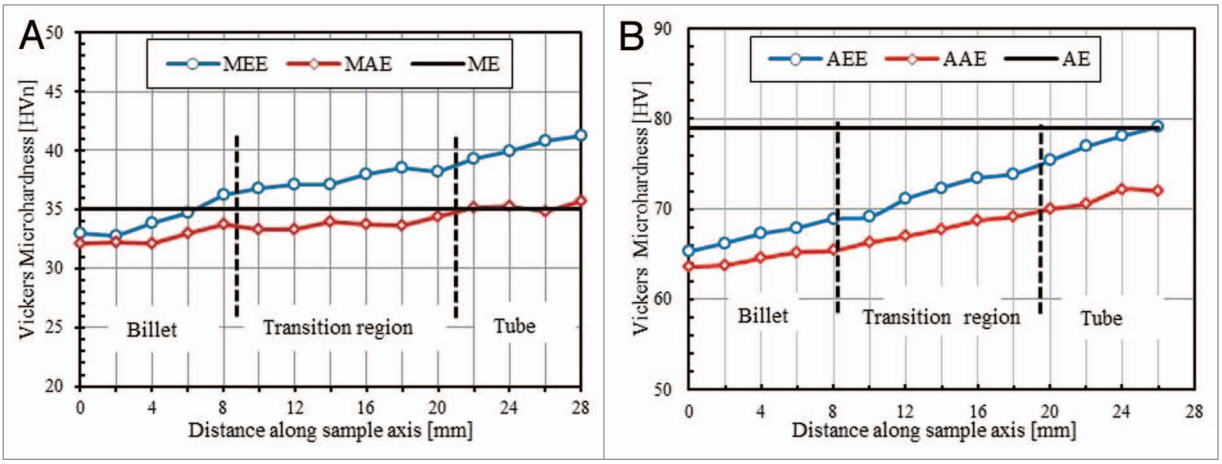

Figure 7. Micro-hardness profiles on longitudinal cross sections of samples subjected to interrupted extrusion tests: Mg (**A**) and ZK60 alloy (**B**).

precisely, a steady-state OCP was observed in the range of –1.7 V vs. Ag/AgCl for pure Mg samples and a second level was observed in the range of –1.5 V vs. Ag/AgCl for ZK60 alloy samples. The 200 mV shift toward more positive potentials reveals a nobler behavior of the alloyed samples, that is believed to be caused by the formation of a protective film of hydroxyapatite (HA) and other Mg/Ca phosphates in SBF.[8]

Apart from the obvious difference between the OCP of alloyed and pure Mg, the as-received samples in both cases showed a slightly nobler behavior when compared with ECAP samples (OCP_{AA}: –1.49V vs. OCP_{AE}: –1.51 $V_{Ag/AgCl}$ and OCP_{MA}: –1.70V vs. OCP_{ME}: –1.725 $V_{Ag/AgCl}$).

Figure 9 shows the the potentiodynamic measurements of all the investigated samples. The same big distinction observed in

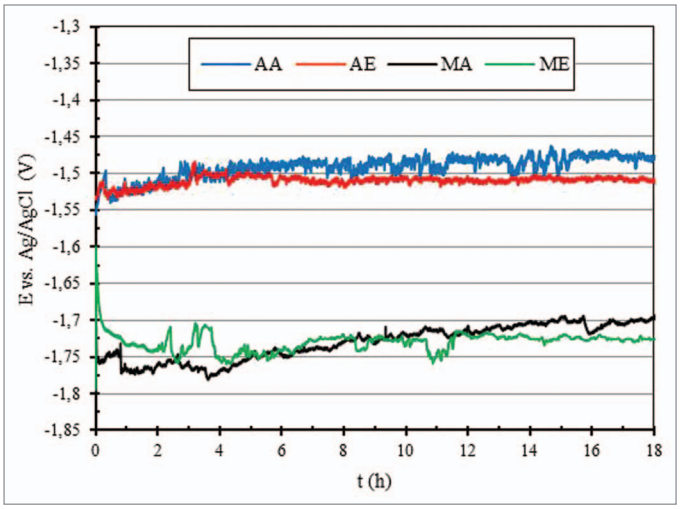

Figure 8. The corrosion potential of pure Mg and ZK60 alloy with time in PBS at 37 °C.

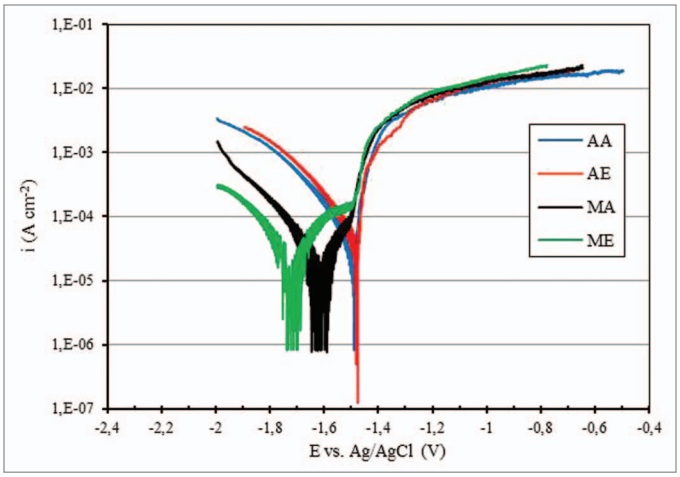

Figure 9. Potentiodynamic polarization curves of pure Mg and ZK60 alloy immersed in PBS before and after ECAP.

OCP results between the alloyed and pure Mg is present here in inversion potentials of the two groups as well. Another significant difference between these two groups of materials can be recognized in the presence of a breakdown potential in the anodic parts of MA and ME samples that is lacking in AA and AE samples. This potential (–1.5 $V_{Ag/AgCl}$ for both MA and ME) at which a sudden "jump" in the corrosion current is observed following a passive-like limited current region, is another sign of the formation of a "protective" layer, that is then broken down at this "pitting" potential.[43,44] In the case of AA and AE samples however, it is seen that the anodic region already started from this pitting potential and hence, the jump is not observed on the curves. In other words, it is supposed that the inversion potential of AA and AE samples roughly coincides with the pitting potential. It is reported in the literature[45] that one of the effects of Zn alloying element on Mg consists of localized corrosion, in the form of pitting corrosion. This observation is in good agreement with the aforementioned anodic behavior observed in the ZK60 samples.

Regarding the corrosion current densities (i_{corr}) estimated from the Tafel extrapolation method, AA and AE samples were found to show similar i_{corr} values, of 60.4 and 56.2 μA cm^{-2}, respectively. These data are higher than those of MA and ME samples (both showing an i_{corr} of 44.7 μA cm^{-2}) suggesting that, although the protective film is more likely to be formed in the alloyed samples, the breakdown of is this layer is inevitable in chlorine-containing environments. Therefore, not only the permanent protection is not provided, but even a faster localized corrosion would happen upon the onset of pitting. Nevertheless, in this case, the gap between the i_{corr} of alloyed and unalloyed samples is not significant. On the other hand, the effect of ECAP treatment on i_{corr} of each group of the samples seems to be modest. Even when considering the MA and ME samples featuring an inversion potential difference of about 100mV (–1.72 and –1.62 $V_{Ag/AgCl}$ for ME and MA, respectively), i_{corr} remains almost constant at 44.7 μA cm^{-2}.

Corrosion morphology

Figures 10 and 11 depict the surface views of the investigated samples after 96 h immersion in PBS solution and following the removal of corrosion products by chromic acid. In both rod and tube samples, a clear difference can be highlighted between the as-received samples of pure Mg and ZK60 alloy (MA vs. AA and MAE vs. AAE). Referring to the discussions given section 3.4.1, increased pitting corrosion is confirmed from surface aspect as well. Moreover, while in case of pure Mg, ECAP treatment does not seem to have a noticeable effect on the corroded microstructure (compare MA to ME in **Fig. 10** and MAE to MEE in **Fig. 11**), for the ZK60 alloy samples, the ECAP effect on the corrosion regime and microstructure seems remarkable (compare AA to AE in **Fig. 10** and AAE to AEE in **Fig. 11**). This phenomenon can be elucidated by considering the role of alloying elements and the related formation of the second phases.

Due to the larger size of intermetallic particles in AA and AAE samples and lower homogeneity for their dispersion in the matrix compared with the ECAP processed samples, it can be reasonably supposed that the micro-galvanic damage is more active in AA and AAE samples,[44] causing the formation deeper corrosion pits.[46,47] On the contrary when a more homogeneous dispersion of the second phase particles arising from the severe plastic deformation induced by ECAP is promoted, a uniform general corrosion regime can occur preferentially over the localized corrosion mechanism.

Experimental Procedure

Materials and ECAP processing

In this investigation, commercial ZK60 (Mg–5.3Zn–0.48Zr, by wt. %) extruded alloy and hot rolled pure magnesium (99.94%) were selected. Cylindrical specimens of 10 mm in diameter with length of 100 mm were machined from the starting materials. The die used for ECAP processing possessed two channels intersecting at an angle of 110° and with an angle of 20° representing the outer arc of curvature. According to well established Iwahashi equation,[48] this geometry generates an

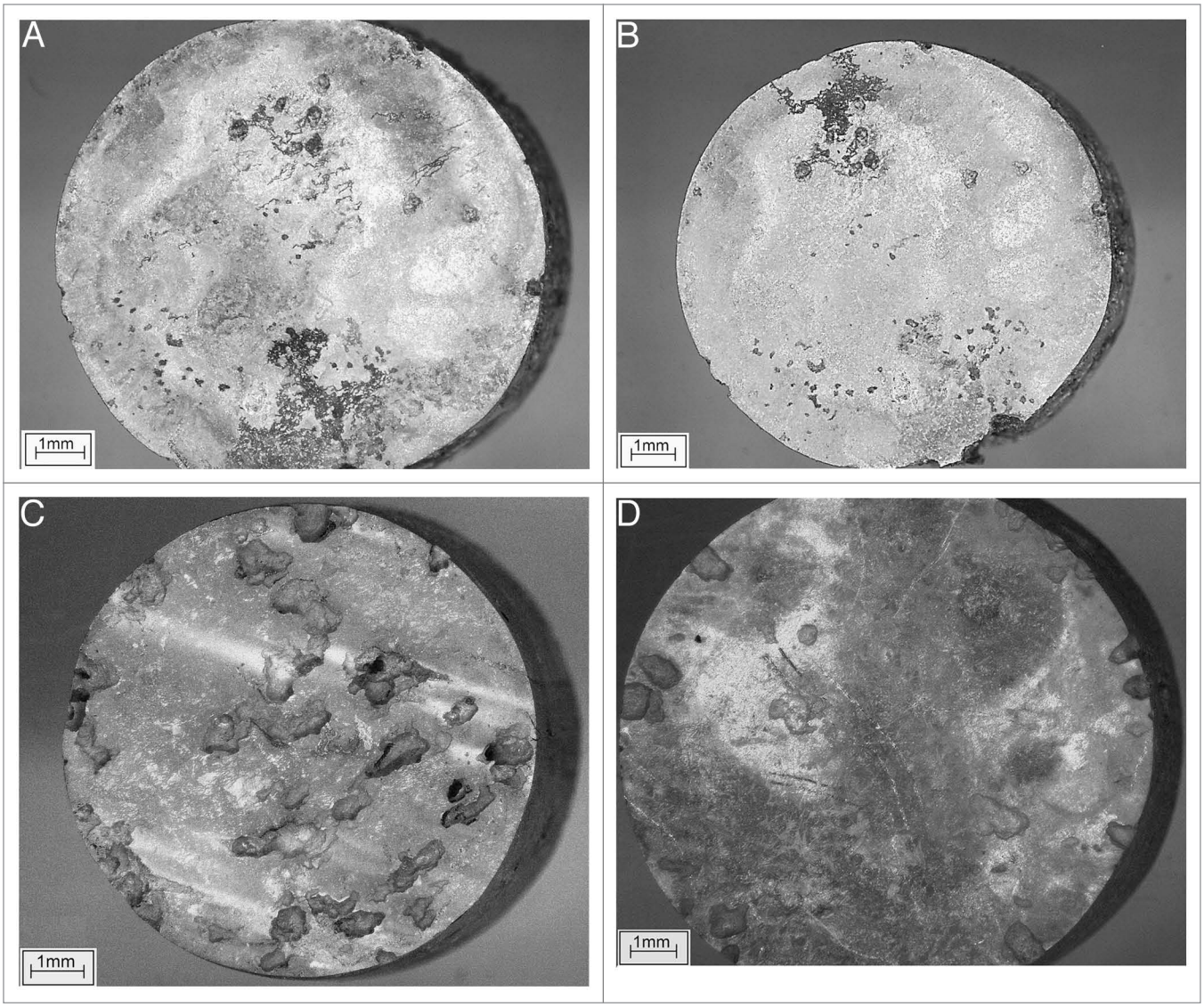

Figure 10. Macrographs of samples immersed in PBS for 96 h: (**A**) MA, (**B**)ME, (**C**)AA, (**D**) AE.

equivalent plastic strain of 0.76 per each pass. The whole die was uniformly heated by 4 electrical resistance heaters distributed along the vertical channel and the temperature was monitored at the intersection points of the channels. All multiple pressings were executed by always rotating the sample in the same direction along the longitudinal axis by 90° before each new pass (route Bc according to established designation given in the literature[49]). Samples were sprayed with MoS_2 lubricant and pressed into the ECAP die at a speed of 30 mm/min. For ZK60 alloy, a first set of ECAP passes was performed at 250 °C for up to 4 passes. Selected specimens were additionally subjected to a second and third set of pressings conducted at 200 °C and 150 °C for other additional 4 passes, at each temperature. For pure magnesium, the first set was performed at 275 °C for 2 passes followed by a second set at 250 °C for 4 passes. Further processing at lower temperature led to extensive cracking and it was therefore abandoned.

Extrusion

Extrusion of ECAP processed materials was performed by using a laboratory device already adopted for coarse grained alloys, described in details in a previous work.[50] Extruded mini-tubes were produced from the ECAP processed billets at temperatures of 150 °C and 230 °C for ZK60 alloy and pure Mg, respectively. The extruded tubes had an outer diameter of 4 mm and an inner diameter of 2.5 mm, corresponding to a reduction ratio of 9:1 performed at a ram speed of 5 mm/min and 2 mm/min for ZK60 and pure Mg, respectively. In order to compare the effects of ECAP on properties of the small size tubes, reference samples of the as received ZK60 alloy and pure Mg were directly extruded at 150 °C and 300 °C, respectively. **Table 1** summarizes the conditions investigated for both materials at the different ECAP and extrusion temperatures.

Microstructural characterization

The specimens for microstructure observation were longitudinally cut (parallel to the ECAP and extrusion direction) ground and polished according to standard metallographic

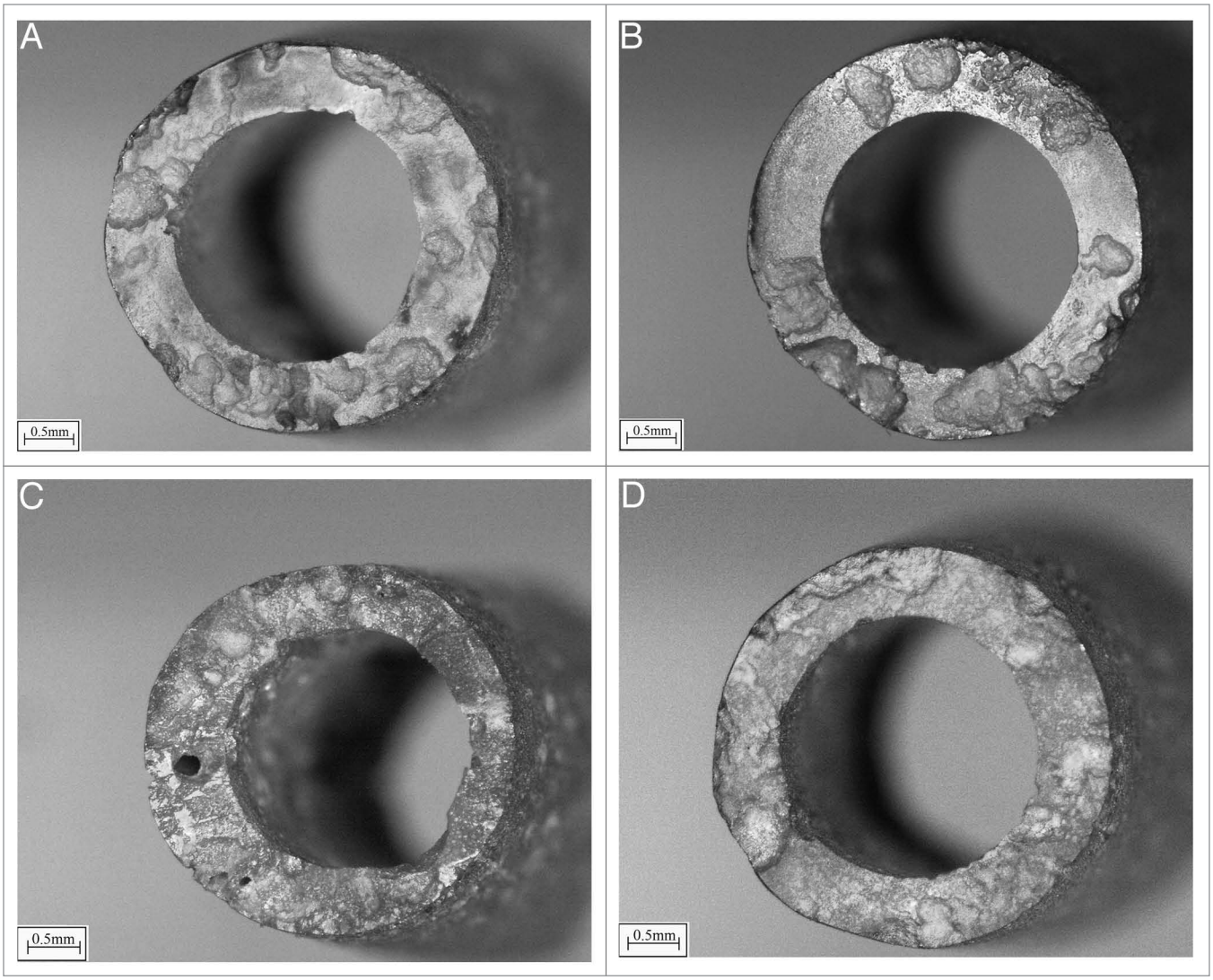

Figure 11. Macrographs of tubes immersed in PBS for 96 h: (**A**) MAE, (**B**)MEE, (**C**)AAE, (**D**) AEE.

procedures. The polished specimens were etched in a solution of 6 g picric acid, 5 ml acetic acid, 10 ml water and 100 ml ethanol. The microstructures of the samples were observed by optical microscopy (OM) and field emission gun scanning electron microscopy (FEG-SEM) on longitudinally cross-sectioned samples after ECAP and extrusion. Characterization of the extruded tubes was comparatively evaluated considering samples extracted from the die after interrupted extrusion trials, where the billet region (thermal effect due to holding at high temperature) and the tube region (combined effects of high temperature and plastic deformation) could be analyzed. The average grain size was evaluated following the procedure given in ASTM E112 standard for the linear intercept method.

Mechanical characterization

Mechanical properties after ECAP process were evaluated by tensile and Vickers microhardness tests. Tensile specimens were machined along the ECAP direction with a gage length of 12 mm and diameter of 4 mm. tensile tests were performed at room temperature at a strain rate of 10^{-3} s^{-1}. Microhardness measurements were made on planes parallel to the extrusion and ECAP directions with an indenter load of 1N. Due to size limitations, the mechanical properties of the extruded tubes were characterized only by Vickers microhardness tests. Measurements were performed on the same samples of the interrupted extrusion trials used for microstructural characterization, where both billet region and tube region could be tested.

Electrochemical measurements

The electrochemical corrosion behavior of MA, AA, ME, and AE samples was studied through open circuit potential (OCP) and potentiodynamic polarization tests. A PTFE sample holder with a circular opening of 5.5 mm diameter was used to isolate the body of the sample from the electrolyte and to provide an electrode area of 23.8 mm^2 in contact with the electrolyte. A phosphate buffer solution (PBS) maintained at 37 °C and pH 7.4 was selected as the electrolyte simulating the body fluid.

A three electrode set up comprised a platinum coated titanium sheet as counter electrode, an Ag/AgCl, Sat. KCl, reference electrode, and different magnesium samples as working

Table 1. ECAP and extrusion processing conditions of the samples investigated.

Sample code	Sample condition
MA	As-received pure Mg
ME	MA ECAP treated for 2 passes at 275 °C+ 4 passes at 250 °C
MEE	ME + extrusion at 230 °C
MAE	MA + extrusion at 300 °C
AA	As-received ZK60 alloy
AE	AA ECAP treated for 3 steps of 4 passes at namely, 250 °C + 200 °C + 150 °C
AEE	AE + extrusion at 150 °C
AAE	AA + extrusion at 150 °C

electrodes. A 7050 AMEL-Potentiostat/Galvanostat was used to perform the experiments. First, OCP was measured for 18 h vs. Ag/AgCl. Then, linear polarization was performed in the potential window of –2 to –0.7 V vs. Ag/AgCl, with a scan rate of 0.166 mV s^{-1}.

Conclusion

The microstructure, mechanical and corrosion properties of ultra-fine grained ZK60 alloy and of pure Mg were investigated in view of the potential application of these materials for biodegradable devices. The conclusion can be summarized as follows:

(1) ECAP process was performed according to a multi-step strategy aimed at achieving a first refining of the structure and then reaching the UFG grain size range by still reducing the processing temperature. A homogeneous equiaxed grain structure with average size in the range of 700 nm was successfully achieved for the ZK60 alloy, while dynamic recrystallization and rapid grain coarsening occurring in commercial pure magnesium prevented the achievement of a grain size smaller than 22 μm.

(2) ECAP process had a considerable influence on the grain size as well as on texture of pure Mg and ZK60 alloy. A combination of texture softening and grain refinement in ECAP processed samples led to excellent mechanical properties with about 100 and 135% improvement in fracture elongation for ZK60 and pure Mg, respectively, while keeping relatively high TYS and UTS values.

(3) ECAP processed ZK60 and pure Mg billets showed better plastic formability than non-ECAP treated samples and therefore, were successfully extruded at 150 and 230 °C, to produce small-size tubes as stent precursors. The UFG structure of ZK60 alloy was maintained also after extrusion due to the contribution of dynamic recrystallization and low processing temperature. At the beginning of the extrusion process, hardness of pure Mg and of ZK60 alloy dropped by warm temperature holding, but was soon recovered due to the refinement promoted by dynamic recrystallization at low processing temperature,

(4) Based on the OCP and potentiodynamic experiments, alloying elements have the substantial effect of modifying the protective surface layer on the free corrosion potential and corrosion current density. This effect provides a sort of nobility action on samples, but second-phase particles formed by the presence of alloying elements also encourage the localized corrosion regime that leads to higher corrosion rates and deep local corrosion damage. ECAP treatment had minor effect on electrochemical measurements of OCP and potentiodynamic tests. However, its main contribution is on the restrictions put on the heterogeneity of microstructure to make a finer and more homogeneous second-phase dispersion and thereby, depressing the localized corrosion pitting.

Disclosure of Potential Conflicts of Interest

No potential conflicts of interest were disclosed.

Acknowledgments

The authors would like to thank Fondazione CaRiTRO for partially funding the research under grant number 2011.0250. Thanks are also due to Dr. N. Hort for supplying the pure Mg and to Dr. A Tuissi and P. Bassani for their support in hot rolling the samples.

References

1. Böstman OM, Pihlajamäki HK. Adverse Tissue Reactions to Bioabsorbable Fixation Devices. Clinical Orthopaedics and Related Research 2000; 371:216-27.
2. Erne P, Schier M, Resink TJ. The road to bioabsorbable stents: reaching clinical reality? Cardiovasc Intervent Radiol 2006; 29:11-6; PMID:16195840; http://dx.doi.org/10.1007/s00270-004-0341-9
3. Moravej M, Mantovani D. Biodegradable metals for cardiovascular stent application: interests and new opportunities. Int J Mol Sci 2011; 12:4250-70; PMID:21845076; http://dx.doi.org/10.3390/ijms12074250
4. Witte F, Hort N, Vogt C, Cohen S, Kainer KU, Willumeit R, Feyerabend F. Degradable biomaterials based on magnesium corrosion. Curr Opin Solid State Mater Sci 2008; 12:63-72; http://dx.doi.org/10.1016/j.cossms.2009.04.001
5. Hermawan H, Dubé D, Mantovani D. Developments in metallic biodegradable stents. Acta Biomater 2010; 6:1693-7; PMID:19815097; http://dx.doi.org/10.1016/j.actbio.2009.10.006
6. Witte F, Kaese V, Haferkamp H, Switzer E, Meyer-Lindenberg A, Wirth CJ, Windhagen H. In vivo corrosion of four magnesium alloys and the associated bone response. Biomaterials 2005; 26:3557-63; PMID:15621246; http://dx.doi.org/10.1016/j.biomaterials.2004.09.049
7. Gu X, Zheng Y, Cheng Y, Zhong S, Xi T. In vitro corrosion and biocompatibility of binary magnesium alloys. Biomaterials 2009; 30:484-98; PMID:19000636; http://dx.doi.org/10.1016/j.biomaterials.2008.10.021
8. Zhang S, Zhang X, Zhao C, Li J, Song Y, Xie C, Tao H, Zhang Y, He Y, Jiang Y, et al. Research on an Mg-Zn alloy as a degradable biomaterial. Acta Biomater 2010; 6:626-40; PMID:19545650; http://dx.doi.org/10.1016/j.actbio.2009.06.028
9. Waksman R, Pakala R, Kuchulakanti PK, Baffour R, Hellinga D, Seabron R, Tio FO, Wittchow E, Hartwig S, Harder C, et al. Safety and efficacy of bioabsorbable magnesium alloy stents in porcine coronary arteries. Catheter Cardiovasc Interv 2006; 68:607-17, discussion 618-9; PMID:16969879; http://dx.doi.org/10.1002/ccd.20727
10. Erbel R, Di Mario C, Bartunek J, Bonnier J, de Bruyne B, Eberli FR, Erne P, Haude M, Heublein B, Horrigan M, et al.; PROGRESS-AMS (Clinical Performance and Angiographic Results of Coronary Stenting with Absorbable Metal Stents) Investigators. Temporary scaffolding of coronary arteries with bioabsorbable magnesium stents: a prospective, non-randomised multicentre trial. Lancet 2007; 369:1869-75; PMID:17544767; http://dx.doi.org/10.1016/S0140-6736(07)60853-8
11. Vormann J. Magnesium: nutrition and metabolism. Mol Aspects Med 2003; 24:27-37; PMID:12537987; http://dx.doi.org/10.1016/S0098-2997(02)00089-4
12. Song G, Atrens A. Understanding Magnesium Corrosion—A Framework for Improved Alloy Performance. Adv Eng Mater 2003; 5:837-58; http://dx.doi.org/10.1002/adem.200310405
13. Song G. Control of biodegradation of biocompatable magnesium alloys. Corros Sci 2007; 49:1696-701; http://dx.doi.org/10.1016/j.corsci.2007.01.001
14. Song G, Song S. A Possible Biodegradable Magnesium Implant Material. Adv Eng Mater 2007; 9:298-302; http://dx.doi.org/10.1002/adem.200600252

15. Song G. Recent Progress in Corrosion and Protection of Magnesium Alloys. Adv Eng Mater 2005; 7:563-86; http://dx.doi.org/10.1002/adem.200500013
16. Song GL. Control of Degradation of Biocompatible Magnesium in a Pseudo-Physiological Environment by a Ceramic Like Anodized Coating. Advanced Materials Research 2007; 29-30:95-8; http://dx.doi.org/10.4028/www.scientific.net/AMR.29-30.95
17. Serruys PW, de Jaegere P, Kiemeneij F, Macaya C, Rutsch W, Heyndrickx G, Emanuelsson H, Marco J, Legrand V, Materne P, et al.; Benestent Study Group. A comparison of balloon-expandable-stent implantation with balloon angioplasty in patients with coronary artery disease. N Engl J Med 1994; 331:489-95; PMID:8041413; http://dx.doi.org/10.1056/NEJM199408253310801
18. Venugopal B, Luckey TD. Metal toxicity in mammals. Volume 2. Chemical toxicity of metals and metalloids. 1978;x + 409pp.
19. Nakamura Y, Tsumura Y, Tonogai Y, Shibata T, Ito Y. Differences in behavior among the chlorides of seven rare earth elements administered intravenously to rats. Fundam Appl Toxicol 1997; 37:106-16; PMID:9242583; http://dx.doi.org/10.1006/faat.1997.2322
20. Yang W, Zhang P, Liu J, Xue Y. Effect of Long-Term Intake of Y3+ in Drinking Water on Gene Expression in Brains of Rats. J Rare Earths 2006; 24:369-73; http://dx.doi.org/10.1016/S1002-0721(06)60126-9
21. StJohn DH, Qian M, Easton MA, Cao P, Hildebrand Z. Grain refinement of magnesium alloys. Metall Mater Trans, A Phys Metall Mater Sci 2005; 36:1669-79; http://dx.doi.org/10.1007/s11661-005-0030-6
22. Goodman SB, Davidson JA, Fornasier VL, Mishra AK. Histological response to cylinders of a low modulus titanium alloy (Ti-13Nb-13Zr) and a wear resistant zirconium alloy (Zr-2.5Nb) implanted in the rabbit tibia. J Appl Biomater 1993; 4:331-9; http://dx.doi.org/10.1002/jab.770040407
23. Chang J, Guo X, He S, Fu P, Peng L, Ding W. Investigation of the corrosion for Mg–xGd–3Y–0.4Zr (x = 6, 8, 10, 12 wt%) alloys in a peak-aged condition. Corros Sci 2008; 50:166-77; http://dx.doi.org/10.1016/j.corsci.2007.06.003
24. Ben-Hamu G, Eliezer D, Shin KS, Cohen S. The relation between microstructure and corrosion behavior of Mg–Y–RE–Zr alloys. J Alloy Comp 2007; 431:269-76; http://dx.doi.org/10.1016/j.jallcom.2006.05.075
25. Orlov D, Ralston KD, Birbilis N, Estrin Y. Enhanced corrosion resistance of Mg alloy ZK60 after processing by integrated extrusion and equal channel angular pressing. Acta Mater 2011; 59:6176-86; http://dx.doi.org/10.1016/j.actamat.2011.06.033
26. Aung NN, Zhou W. Effect of grain size and twins on corrosion behaviour of AZ31B magnesium alloy. Corros Sci 2010; 52:589-94; http://dx.doi.org/10.1016/j.corsci.2009.10.018
27. Valiev RZ, Langdon TG. Principles of equal-channel angular pressing as a processing tool for grain refinement. Prog Mater Sci 2006; 51:881-981; http://dx.doi.org/10.1016/j.pmatsci.2006.02.003
28. Yamashita A, Horita Z, Langdon TG. Improving the mechanical properties of magnesium and a magnesium alloy through severe plastic deformation. Mater Sci Eng A 2001; 300:142-7; http://dx.doi.org/10.1016/S0921-5093(00)01660-9
29. Alvarez-Lopez M, Pereda MD, del Valle JA, Fernandez-Lorenzo M, Garcia-Alonso MC, Ruano OA, Escudero ML. Corrosion behaviour of AZ31 magnesium alloy with different grain sizes in simulated biological fluids. Acta Biomater 2010; 6:1763-71; PMID:19446048; http://dx.doi.org/10.1016/j.actbio.2009.04.041
30. Ge Q, Dellasega D, Demir AG, Vedani M. The processing of ultrafine-grained Mg tubes for biodegradable stents. Acta Biomater 2013; 9:8604-10; PMID:23333440; http://dx.doi.org/10.1016/j.actbio.2013.01.010
31. Li J, Xu W, Wu X, Ding H, Xia K. Effects of grain size on compressive behaviour in ultrafine grained pure Mg processed by equal channel angular pressing at room temperature. Mater Sci Eng A 2011; 528:5993-8; http://dx.doi.org/10.1016/j.msea.2011.04.045
32. Tong LB, Zheng MY, Hu XS, Wu K, Xu SW, Kamado S, Kojima Y. Influence of ECAP routes on microstructure and mechanical properties of Mg–Zn–Ca alloy. Mater Sci Eng A 2010; 527:4250-6; http://dx.doi.org/10.1016/j.msea.2010.03.062
33. Ding R, Chung C, Chiu Y, Lyon P. Effect of ECAP on microstructure and mechanical properties of ZE41 magnesium alloy. Mater Sci Eng A 2010; 527:3777-84; http://dx.doi.org/10.1016/j.msea.2010.02.030
34. Li S. Orientation stability in equal channel angular extrusion. Part II: Hexagonal close-packed materials. Acta Mater 2008; 56:1031-43; http://dx.doi.org/10.1016/j.actamat.2007.11.003
35. Lin HK, Huang JC, Langdon TG. Relationship between texture and low temperature superplasticity in an extruded AZ31 Mg alloy processed by ECAP. Mater Sci Eng A 2005; 402:250-7; http://dx.doi.org/10.1016/j.msea.2005.04.018
36. Seipp S, Wagner MF-X, Hockauf K, Schneider I, Meyer LW, Hockauf M. Microstructure, crystallographic texture and mechanical properties of the magnesium alloy AZ31B after different routes of thermo-mechanical processing. Int J Plast 2012; 35:155-66; http://dx.doi.org/10.1016/j.ijplas.2012.03.007
37. Kim WJ, Hong SI, Kim YS, Min SH, Jeong HT, Lee JD. Texture development and its effect on mechanical properties of an AZ61 Mg alloy fabricated by equal channel angular pressing. Acta Mater 2003; 51:3293-307; http://dx.doi.org/10.1016/S1359-6454(03)00161-7
38. Koike J, Kobayashi T, Mukai T, Watanabe H, Suzuki M, Maruyama K, Higashi K. The activity of non-basal slip systems and dynamic recovery at room temperature in fine-grained AZ31B magnesium alloys. Acta Mater 2003; 51:2055-65; http://dx.doi.org/10.1016/S1359-6454(03)00005-3
39. Agnew SR, Horton JA, Lillo TM, Brown DW. Enhanced ductility in strongly textured magnesium produced by equal channel angular processing. Scr Mater 2004; 50:377-81; http://dx.doi.org/10.1016/j.scriptamat.2003.10.006
40. Mani G, Feldman MD, Patel D, Agrawal CM. Coronary stents: a materials perspective. Biomaterials 2007; 28:1689-710; PMID:17188349; http://dx.doi.org/10.1016/j.biomaterials.2006.11.042
41. Matsubara K, Miyahara Y, Horita Z, Langdon TG. Developing superplasticity in a magnesium alloy through a combination of extrusion and ECAP. Acta Mater 2003; 51:3073-84; http://dx.doi.org/10.1016/S1359-6454(03)00118-6
42. Horita Z, Matsubara K, Makii K, Langdon TG. A two-step processing route for achieving a superplastic forming capability in dilute magnesium alloys. Scr Mater 2002; 47:255-60; http://dx.doi.org/10.1016/S1359-6462(02)00135-5
43. Song G, Atrens A, Wu X, Zhang B. Corrosion behaviour of AZ21, AZ501 and AZ91 in sodium chloride. Corros Sci 1998; 40:1769-91; http://dx.doi.org/10.1016/S0010-938X(98)00078-X
44. Atrens A, Liu M, Zainal Abidin NI. Corrosion mechanism applicable to biodegradable magnesium implants. Mater Sci Eng B 2011; 176:1609-36; http://dx.doi.org/10.1016/j.mseb.2010.12.017
45. Shi Z, Song G, Atrens A. Corrosion resistance of anodised single-phase Mg alloys. Surf Coat Tech 2006; 201:492-503; http://dx.doi.org/10.1016/j.surfcoat.2005.11.081
46. Song GL, Atrens A. Corrosion Mechanisms of Magnesium Alloys. Adv Eng Mater 1999; 1:11-33; http://dx.doi.org/10.1002/(SICI)1527-2648(199909)1:1<11::AID-ADEM11>3.0.CO;2-N
47. Zeng R, Kainer KU, Blawert C, Dietzel W. Corrosion of an extruded magnesium alloy ZK60 component—The role of microstructural features. J Alloy Comp 2011; 509:4462-9; http://dx.doi.org/10.1016/j.jallcom.2011.01.116
48. Iwahashi Y, Wang J, Horita Z, Nemoto M, Langdon TG. Principle of equal-channel angular pressing for the processing of ultra-fine grained materials. Scr Mater 1996; 35:143-6; http://dx.doi.org/10.1016/1359-6462(96)00107-8
49. Segal VM. Equal channel angular extrusion: from macromechanics to structure formation. Mater Sci Eng A 1999; 271:322-33; http://dx.doi.org/10.1016/S0921-5093(99)00248-8
50. Ge Q, Vedani M, Vimercati G. Extrusion of Magnesium Tubes for Biodegradable Stent Precursors. Mater Manuf Process 2012; 27:140-6; http://dx.doi.org/10.1080/10426914.2011.560231